Time-Dependent Stokes Shifts of Fluorescent Dyes in the Hydrophobic Backbone Region of a Phospholipid Bilayer: Combination of Fluorescence Spectroscopy and Ab Initio Calculations

Jan Sýkora,*,† Petr Slavíček,*,†,‡ Pavel Jungwirth,§ Justyna Barucha,† and Martin Hof†

J. Heyrovský Institute of Physical Chemistry, Academy of Sciences of the Czech Republic, Dolejškova 3, 18223 Prague 8, Czech Republic, Department of Physical Chemistry, Prague Institute of Chemical Technology, Technická 5, 16628 Prague 6, Czech Republic, and Institute of Organic Chemistry and Biochemistry, Academy of Sciences of the Czech Republic, and Center for Biomolecules and Complex Molecular Systems, Flemingovo nám. 2, 16610 Prague 6, Czech Republic

Received: March 9, 2007

We explored the time-dependent Stokes shifts of fluorescent dyes containing an anthroyloxy chromophore (2-AS, 9-AS, and 16-AP) in bilayers composed of palmitoyl-oleoyl-phosphatidylcholine. The obtained data revealed a nontrivial solvation response of these dyes, which are located in the backbone region of the bilayer with a gradually increasing depth. For comparison, steady-state emission spectra in the neat solvents of various polarities and viscosities were also recorded. The results indicate that on the short picosecond time scale the AS dyes undergo complex photophysics including formation of states with a charge-transfer character. This observation is supported by ab initio calculations of the excited states of 9-methylanthroate. The slower nanosecond part of the relaxation process can be attributed to the solvation response of the dyes. A slowdown in solvent relaxation is observed upon moving toward the center of the bilayer. A mechanism similar to preferential solvation present in the mixture of a polar and nonpolar solvent is considered to explain the obtained data.

1. Introduction

Hydration of biological molecules and self-assemblies enables their proper functioning and enhances their stability. Water molecules present in the hydration layer have been proven to have completely different intermolecular structure and dynamical properties compared to the bulk solution. For instance, solvation dynamics are slowed down remarkably.[1] Phospholipid bilayers, which form a basic part of cellular membranes, belong to the most important biological systems. With respect to their structure we distinguish two main regions within the bilayer: the interface and the backbone region.[2,3] The interface region includes hydrated phosphate, glycerol, and carbonyl groups. Here, solvation dynamics take place on a rather broad time scale (with reported picosecond, subnanosecond, and up to nanosecond components).[4−6] The intrinsic thermal fluctuations in the bilayer and the spread of chromophore locations leads to a broad distribution of different microenvironments and thus to the observed "unspecific" solvent relaxation (SR) dynamics. However, as the interface is chemically highly heterogeneous, some dyes located at/close to the carbonyl groups show quite homogeneous solvation response, which occurs exclusively on the nanosecond time scale.[5,7] This part of the bilayer interface will be reffered to as the "headgroup region" further in the text. As indicated above, the interface represents a rather heterogeneous and dynamic structure comprising the hydrated and charged chemical residues, which makes the application of molecular dynamics (MD) simulation for explaining the observed nanosecond kinetics rather difficult.[8]

The backbone region is composed of the hydrophobic chains of fatty acids where the water content was found to be low.[9] The only fluorescent dyes suitable for monitoring the solvation dynamics in this region are presently the probes with the anthroyloxy ring attached to the fatty acid chain at various positions (known as *n*-AS dyes) (Figure 1). These probes were reported to be located at a well-defined graded series of depths along the normal axis of the bilayer.[10,11] It has been known for a long time that anthroyloxy-based dyes can serve as sensitive polarity probes.[10−15] It is, therefore, possible to use *n*-AS for investigating the water concentration profile and for probing the dynamics of water in the backbone region of the phospholipid bilayer.

An important insight into the nature of solvation dynamics can be provided by MD simulations. These were applied for studies of, for example, chromophores dissolved in a polar solvent[16] or at the liquid/liquid interfaces,[17] chromophores located in a mixture of polar and nonpolar solvents,[18] or in polar nanoclusters.[19] The latter two cases are specifically important for the discussion of solvation dynamics in the backbone region of the bilayer. In both cases the chromophore is incompletely solvated by the polar solvent. Molecular dynamics studies lead the to identification of different solvation time scales connected with different molecular motions, starting from a femtosecond time scale for the librational solvent response, over a picosecond time scale for solvent rearrangements around the chromophore,

* Authors to whom correspondence should be addressed. E-mail: jan.sykora@jh-inst.cas.cz; petr.slavicek@vscht.cz.

† J. Heyrovský Institute of Physical Chemistry, Academy of Sciences of the Czech Republic.

‡ Prague Institute of Chemical Technology.

§ Institute of Organic Chemistry and Biochemistry, Academy of Sciences of the Czech Republic, and Center for Biomolecules and Complex Molecular Systems.

10.1021/jp0719255 CCC: $37.00
Published on Web 05/08/2007

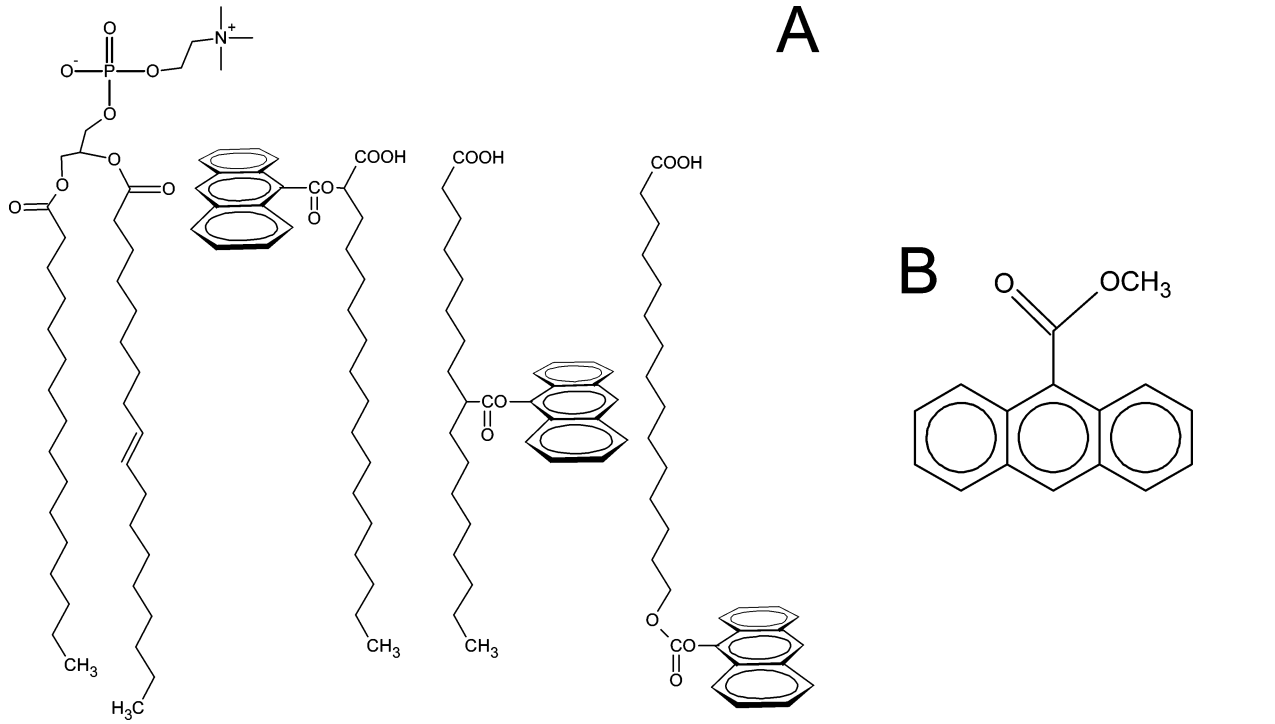

Figure 1. (A) Schematic structures of POPC, 2-AS, 9-AS, and 16-AP. Approximate localization of the *n*-AS dyes relative to the lipid molecules are depicted. (B) Structure of 9-methylanthroate (9MA).

up to the nanosecond diffusion component corresponding to the flow of the solvent molecules toward/from the excited chromophore.

The goal of this work is to probe solvation dynamics by recording the time-resolved emission spectra (TRES) in varying depths of the backbone region of the bilayer. Large unilamellar vesicles (LUVs) composed of 1-palmitoyl-2-oleoyl-phosphatidylcholine (POPC) lipid molecules are used as a model system. The inspection of the TRES is supposed to bring new insights into the properties and structure of the water molecules present in the labeled regions. However, the TRES contain information not only about the solvation dynamics but potentially also about intramolecular processes. In the case of AS dyes, the photophysics are rather complex and still not fully understood. It has, for example, never been fully satisfactorily explained why the fluorescence behavior of anthroyloxy-based dyes is strongly solvent-dependent. Detailed understanding of the intramolecular dynamics of the respective dyes is, however, vital for a correct interpretation of the TRES. To this end, the present experiments on 2-AS, 9-AS, and 16-anthroyloxy-palmitoic acid (16-AP) are also accompanied by data collected at various temperatures in different solvents of varying polarities and viscosities. The aim is to obtain a more thorough understanding of the photophysics of these dyes, which enables interpretation of the results gained from TRES.

In addition, the photophysics of the dyes are rationalized by means of quantum mechanical calculations on a smaller model system of 9-methylanthroate. Results of theoretical calculations allow us to understand the time-dependent fluorescence behavior of anthroyloxy dyes, assigning different processes to individual time scales.

The paper is organized as follows. In section 2, the employed experimental and theoretical methods are described. Results together with a discussion are presented in the third section. Section 4 concludes the paper with an outlook for future studies.

2. Materials and Methods

2.1. Experimental Methods. All probes, (2-(9-anthroyloxy)-stearic acid (2-AS), 9-(9-anthroyloxy)stearic acid (9-AS), 16-(9-anthroyloxy)palmitic acid (16-AP)), Figure 1, and 6-hexadecanoyl-2-(((2-(trimethylammonium)ethyl)methyl)amino)naphthalene chloride (Patman) were purchased from Molecular Probes and were used without any further purification. Phospholipids (1-palmitoyl-2-oleoyl-phosphatidylcholine (POPC) and dipalmitoylphosphatidylcholine (DPPC)) were supplied from Avanti Lipids. All solvents of spectroscopic grade were purchased from Merck. The preparation of DPPC and POPC LUVs was performed as described previously by extruding with 100 nm filters.[20] Absorption spectra were recorded on a Perkin-Elmer Lambda 19 spectrometer. Fluorescence spectra and decays were recorded on a Fluorolog 3 steady-state spectrometer (Jobin Yvon) and on IBH 5000 U SPC equipment. The experimental temperature was set to 27 °C, unless stated differently. Low-temperature steady-state spectra were measured on a modified Edinburgh Instruments FLFS900 spectrometer. Decay kinetics were recorded using an IBH Nanoled 11 excitation source (370 nm peak wavelength, 80 ps pulse width, 1 MHz repetition rate) and a cooled Hamamatsu R3809U-50 microchannel plate photomultiplier. The primary data consisted of a set of emission decays recorded at a series of wavelengths spanning the steady-state emission spectrum. The TRES's were obtained by the spectral reconstruction method.[21] Full width at half-maximum (fwhm(t)) and emission maxima ($\nu(t)$) profiles of the reconstructed TRES were obtained by a log-normal fitting.[21] The correlation functions $C(t)$ were calculated according to

$$C(t) = \frac{\nu(t) - \nu(\infty)}{\nu(0) - \nu(\infty)} \quad (1)$$

where $\upsilon(0)$ and $\upsilon(\infty)$ correspond to the value obtained by "time 0 estimation" and to the value at time infinity, respectively. The

kinetics of the solvation dynamics were parametrized with the so-called relaxation times τ_r

$$\tau_r = \int_0^\infty C(t)\, dt \qquad (2)$$

Generally, in the studies investigating solvation dynamics the solvent relaxation time, τ_{SR}, which is defined as an integral of the correlation function, describes the kinetics of SR quantitatively. We define above the integral relaxation time τ_r, which is analogous to the SR time. However, it characterizes the time course of the overall relaxation process including both the internal intramolecular relaxation and solvent relaxation and thus gives only limited information on the individual processes leading to a time-dependent shift in the emission spectra.

2.2. Computational Methods. We have performed electronic structure calculations to investigate possible photochemical mechanisms. Several levels of description have been employed. For entry level calculations the semiempirical AM1 Hamiltonian has been utilized. To deal with excited states, the FOMO-CAS-(6/6) scheme has been used.[22] Since the semiempirical parametrization is not adequate to describe the potential energy surface far from the equilibrium geometries, we have used ab initio techniques to address this issue. The ground-state minimum of the investigated dye (9-methylanthroate) has been obtained at the MP2/6-31g* level. For exploration of the potential energy surfaces of the excited states, we have used the complete active space self-consistent field (CAS-SCF) method with an active space consisting of six electrons in six orbitals with the same basis set as above. At this level we have also performed excited-state geometry optimization. At the optimized geometries we have performed single-point CASPT2 calculations. During the CASPT2 calculations, 40 orbitals have been kept frozen to make the calculation numerically feasible. The results are, however, not particularly sensitive to the exact number of orbitals kept frozen. The calculations are essentially stable with respect to change of the active size and the number of states over which we average the energy during the orbital optimization.

All of the CAS-SCF and CASPT2 calculations have been performed with the MOLPRO electronic code package.[23] The semiempirical calculations have been performed with the modified version of the MOPAC package.[24]

3. Results and Discussion

In this section we discuss first the photophysics of the AS dyes on the basis of the absorption and steady-state fluorescence spectra. Consequently, interpretation of the spectra is then deduced from ab initio calculations. Second, we investigate the TRES's measured in the backbone region of the phospholipid bilayer. Solvation and intramolecular dynamics of the AS dyes in biomembranes are then discussed in the context of the present findings about their photophysics.

3.1. Absorption and Excitation Spectra in Different Environments. Absorption and excitation spectra were measured for the set of *n*-(9-AS) ($n = 2, 9$) and 16-(9-AP) dyes in a wide range of solvents and in POPC and DPPC LUVs. All recorded spectra show features characteristic for anthracene with three well-distinguished peaks corresponding to the 0−2, 0−1, and 0−0 transitions. (The numbers stand for the vibrational levels in the ground and excited states, respectively.[25]) The obtained values for the three main peaks of the excitation and absorption spectra are identical for all measured systems within the experimental error of 50 cm^{-1}. Maxima of excitation spectra of 2-AS are summarized in Table 1 for selected solvents and lipid systems. Only a small shift of a maximal value of 200 cm^{-1} is detected for a large range of solvents and vesicle systems. Table 2 shows the values of the middle peak maxima of the excitation spectra for the set of *n*-(9-AS) ($n = 2, 9$) and 16-(9-AP). Again, the excitation spectra and the absorption spectra (not shown here) appear to be largely invariant within the whole set of these compounds. In summary, the absorption and excitation spectra depend neither on the chromophore environment nor on the position of attachment of the fatty acid chain.

TABLE 1: Maxima of Excitation Spectra in 2-AS in Various Systems[a]

solvent	ν_1 (cm^{-1})	ν_2 (cm^{-1})	ν_3 (cm^{-1})
heptane	26 340	27 700	29 150
paraffin oil	26 150	27 550	28 900
propanol	26 200	27 600	28 970
ethanol + methanol	26 240	27 700	29 000
DPPC LUV (25 °C)	26 100	27 470	28 910
DPPC LUV (46 °C)	26 100	27 490	28 960
POPC LUV	26 080	27 500	28 990

[a] The three columns correspond to the three main peaks as described in the text.

TABLE 2: Maxima of Excitation Spectra of "AS Dyes" in Various Systems[a]

solvent	2-AS ν_2 (cm^{-1})	9-AS ν_2 (cm^{-1})	16-AP ν_2 (cm^{-1})
heptane	27 700	27 700	27 760
paraffin oil	27 550	27 550	27 550
propanol	27 600	27 620	27600
ethanol + methanol	27 700	27 700	27 680
POPC LUV	27 500	27 520	27 540

[a] The middle peak (υ_2) of the excitation spectrum is taken into account.

3.2. Fluorescence Emission Spectra. In contrast to the absorption and excitation spectra, both shape and position of the emission steady-state spectra show significant differences when modifying the polarity and viscosity of the solvent.

In nonpolar solvents, on one hand, there are at least two fluorescence bands apparent in the steady-state spectra indicating contributions from at least two energetically different fluorescent states (Figure 2A). Moreover, with the increase of viscosity the peak corresponding to the more energetic state becomes more pronounced, as is obvious for the data recorded in paraffin oil (Figure 2B). On the other hand, in polar solvents, the steady-state spectra lose their fine structure, and particular bands are no longer recognizable (Figure 3A). In addition, the spectra are broadened and red-shifted in contrast to the nonpolar solvents. In both the polar and the nonpolar environments, the recorded fluorescence spectra do not bear the mirror image relation to the absorption spectra. Apart from the dependence of the fluorescence spectra on the polarity and viscosity, an effect of the position of the anthroyloxy group can be observed.

In POPC vesicles the steady-state spectra of 2-AS and 9-AS are rather similar to those observed in polar solvents. In addition, they show the expected trend, and the deeper location of the dye leads to a slight blue shift of the emission spectrum possibly due to the polarity gradient within the bilayer (Figure 3B). In contrast, the character of the fluorescence spectrum for 16-AP is more similar to that observed in a nonpolar environment having an additional discrete band at a lower wavelength. In addition, it is red-shifted in comparison to the steady-state spectra recorded for 9-AS. This fact may be explained by inspecting TRES (section 3.5). Bearing in mind that the observed steady-state spectrum is actually a sum of the TRES and that 16-AP shows the fastest relaxation process of all three

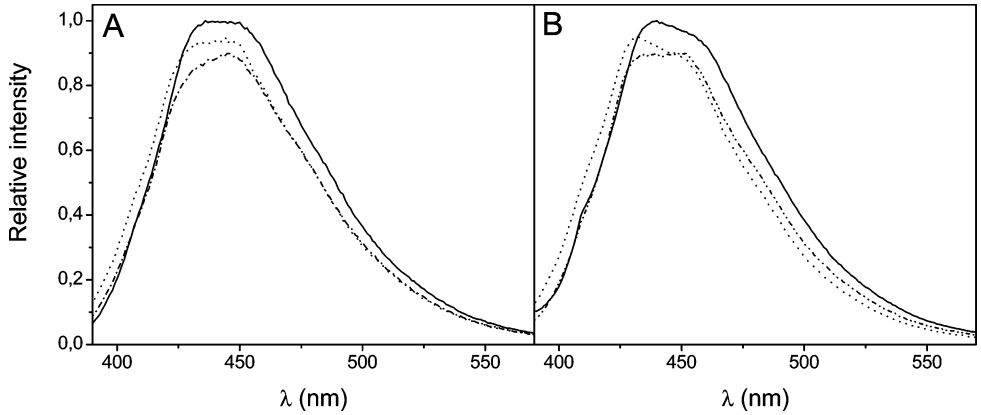

Figure 2. Emission spectra of AS dyes in (A) heptane and (B) paraffin oil: solid line, 2-AS; dotted line, 9-AS; dash−dotted line, 16-AP.

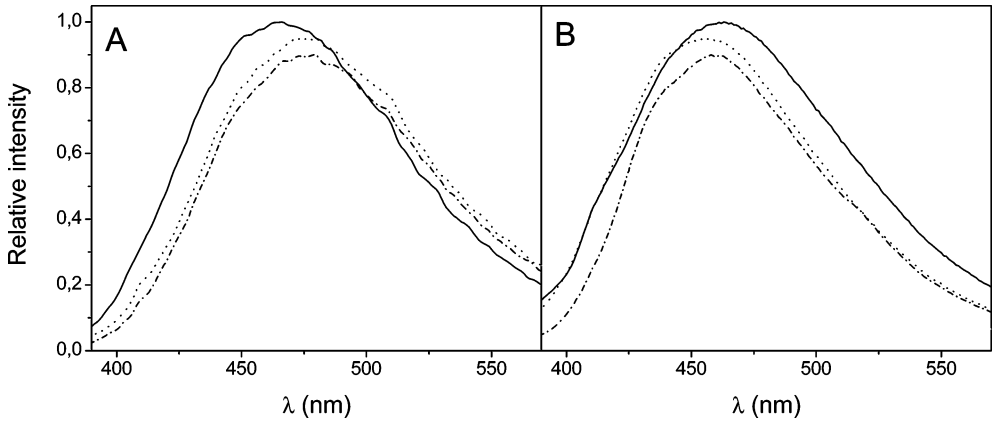

Figure 3. Emission spectra of AS dyes in (A) ethanol−methanol mixture (1:1) and (B) POPC LUVs: solid line, 2-AS; dotted line, 9-AS; dash−dotted line, 16-AP.

dyes (section 3.5), it is obvious that the more relaxed (i.e., more red-shifted) states contribute to the steady-state spectrum more markedly than in the case of 9-AS.

3.3. Quantum Chemical Calculations and the Discussion of the *n*-AS Photophysics. To gain further insight into the photophysics of the *n*-AS dyes, we have explored the excited-state potential energy surface of 9-methylanthroate (9MA) by means of quantum chemical methods. The 9MA molecule (Figure 1B) lacks the long alkyl chain and carboxylic group of the *n*-AS molecules, but it has the same anthracene-based chromophore, capped with a methyl group. It is, therefore, an excellent model system for this type of compound. The emission spectra of *n*-AS dyes and their dependence on the solvent polarity, viscosity, and temperature are qualitatively identical to those of 9MA.

Experimental information for this molecule is available both for different solvents and for an isolated molecule in the gas phase. The 9MA molecule has been studied experimentally in the condensed phase[12,26,27] and in supersonic jets.[28] Semiempirical calculations also have been performed on this molecule.[14]

The absorption spectra of this molecule exhibit anthracene-like structure with a negligible solvent shift. This is in accord with the fact that both the ground- and the excited-state dipole moments are rather low. The fluorescence spectra of 9MA are, on the other hand, strongly red-shifted and diffuse. The Stokes shift is highly solvent-dependent. The dipole moment change estimated from the Lippert−Mataga equation provides a value of 4.5 D.[12] The fluorescence spectra do not bear the mirror image relation with the absorption spectra for any solvent. The above features are also true for the 9MA molecule in the gas phase. Any suggested photochemical scheme of the 9MA dye has to explain those features as well as the polarity, temperature, and viscosity dependence of the *n*-AS fluorescence spectra.

The absence of the mirror image relation of the fluorescence and absorption spectra in the nonpolar solvents and even in the gas phase clearly indicates that a significant intramolecular relaxation takes place upon photoexcitation, which also holds true for AS dyes embedded in the membrane.[29] Two possible mechanisms can be considered: (1) conformational relaxation along the twisting coordinate or (2) formation of different structures, some of them of a charge-transfer character.

The first mechanism has been suggested by Swayanbunathan and Lim[28] for the 9MA molecule and further used by Berberan-Santos and co-workers[13] to rationalize the photophysics of the 12-AS molecule. According to this explanation, the absorption occurs mainly from the twisted configuration that is not preferential for the excited state. As a result, the excited chromophore starts to relax by intramolecular rotation. The increasing viscosity of the environment slows down the intramolecular rotation and leads to emission from initial or partially relaxed states, resulting in the growth of the blue-shifted shoulder of the steady-state spectrum. There are, however, some difficulties with this idea. By looking at the steady-state spectra in heptane and in viscous paraffin oil (Figures 2A and 2B) of all *n*-AS dyes and by inspecting the temperature scan of 2-AS in heptane from 300 to 150 K (Figure 4A) we can safely distinguish at least two emitting states. It is unclear how such a feature could be produced by an emission from a single well. The intramolecular relaxation should also be in this case much faster than that observed in the time-resolved fluorescence

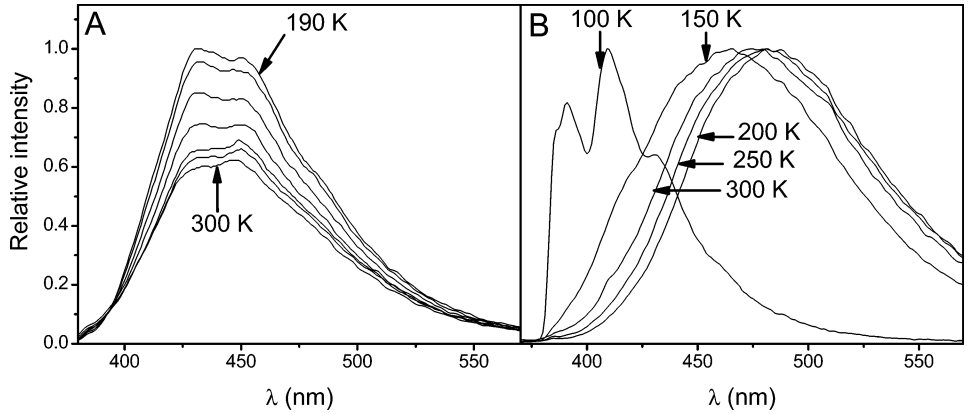

Figure 4. Temperature scan of emission spectra of 2-AS dyes in (A) heptan (spectra recorded at 300, 280, 260, 240, 220, 200, 190 K and the intensity increases with decreasing temperature monotonously) and (B) ethanol−methanol mixture (1:1).

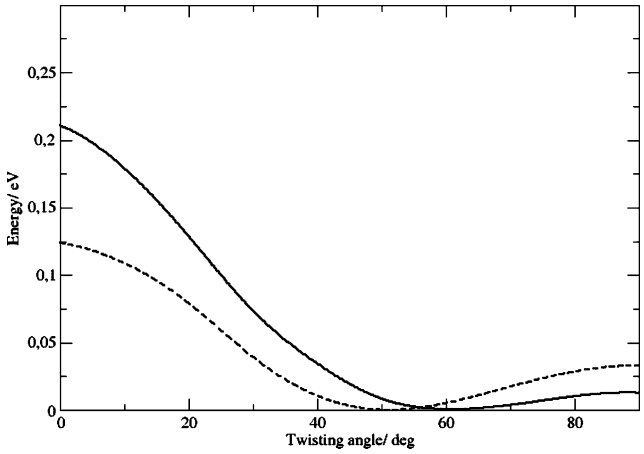

Figure 5. Relaxed torsional potentials for S_0 and S_1 states of 9-methylanthroate calculated at the AM1-FOMO-6/6 level. Full line corresponds to the S_0 state, while the dashed line corresponds to the S_1 state. The S_1 potential has been shifted by −3.2 eV.

experiments. The rotational relaxation mechanism does not explain why such a modest rearrangement could destroy the mirror image character of the fluorescence spectrum. As a matter of fact, the fluorescence spectrum of an analogous methylester of the 9-acridencarboxylic acid in tetrahydrofuran does not exhibit the broad, red-shifted spectrum of 9MA even though the torsional potential in both S_0 and S_1 states and their absorption spectra are very similar.[30]

Further evidence against the rotational relaxation mechanism comes from the present electronic structure calculations. The first excited state in the Franck−Condon region is essentially the anthracene ring $\pi\pi^*$ state. This is a nonpolar state, with a dipole moment being within 1 D from its ground-state value. The torsional curves calculated with a semiempirical AM1 Hamiltonian for the S_0 and S_1 states are depicted in Figure 5. The twisting angle in the ground state is 60°; in the S_1 relaxed state it is 50°. (CAS-SCF optimization provides similar numbers of 58° and 53.5° for the two states.) The barrier at 90° in the S_0 state is less than 0.02 eV; thus it is thermally accessible, the barrier in the S1 state being also low (0.04 eV). This is in good agreement with previous calculations of Dey[30] for a free acid, and the height of the barrier also agrees with the experimental estimate of Swayanbunathan.[28] The Stokes shift between the Franck−Condon point and the relaxed locally excited-state minimum is less than 0.3 eV. These semiempirical calculations are also in a semiquantitative agreement with CAS-SCF and CASPT2 calculations (Table 3). The dipole moment does not change significantly along the rotational coordinate. Neither the value of the Stokes shift nor the solvent dependence is, therefore, in agreement with the rotational relaxation mechanism.

TABLE 3: Characterization of Important Minima on the S_1 Potential Energy Surface of the 9MA Molecule[a]

	FC	LE	Min1	Min2	Min3
CAS/eV	0	−0.6	−0.45	−0.8	−0.7
S0/S1 gap/eV	4.7	4.25	3.3	1.9	1.8
CASPT2/eV	0	0.05	−0.2	0.4	0.85
S0/S1 gap/eV	4.2	3.91	2.6	1.9	2.5
GS dipole/D	1.9	2.0	2.1	3.3	2.1
ES dipole/D	2.3	1.9	6.5	2.1	1.1
transition dipole/D	0.38	0.65	3.4	0.12	0.27

[a] FC denotes the Franck−Condon point, LE is a locally excited state, and Min1−3 are other local minima. Energies at the CAS-SCF(6/6) and corresponding CASPT2 levels are displayed in electronvolts, relative to the FC point.

We thus addressed the question of whether there is a different geometry on the S_1 potential energy surface that would be energetically accessible, possibly lower in energy than the locally excited state. Such a structure should be of a charge-transfer character (and should, therefore, have a large dipole moment) to explain the observed polarity dependence. The search for these local minima has been performed using the CAS-SCF method with the results are summarized in Table 3 and in Figure 6. The potential energy surface of the 9MA molecule in its first excited state is rather complex. We may anticipate that for different atomic configurations the S_1 state will be dominated by configurations with a $\pi\pi^*$ transition localized in the ring, $\pi\pi^*$ transition within the COOMe moiety, $n\pi^*$ transition, or the charge-transfer $\pi\pi^*$ transition. We have localized several distinct minima on the S_1 potential energy surface with energy below or comparable with that of the locally excited (LE) state (Figure 6). These minima are denoted as Min1, Min2, and Min3. Min1 corresponds to a S_1 state minimum with a large dipole moment (6.5 D). This fits nicely with the estimate of a 9MA dipole moment change by Werner.[12] Also the estimated emission wavelength from this structure, 470 nm at the CASPT2 level, and large transition dipole moment for the emission from this state support the idea that we observe this structure in the fluorescence emission spectra. Note also that the charge-transfer (CT) state found here is further stabilized in polar solvents. Geometrically, this structure has a bent anthracene ring with a ring carbon atom connected to the out-of-plane carbonyl group. The anthracene ring in this structure is bent by 25°. There is a single bond between the carboxylic carbon and the anthracene group while the C═O bond remains

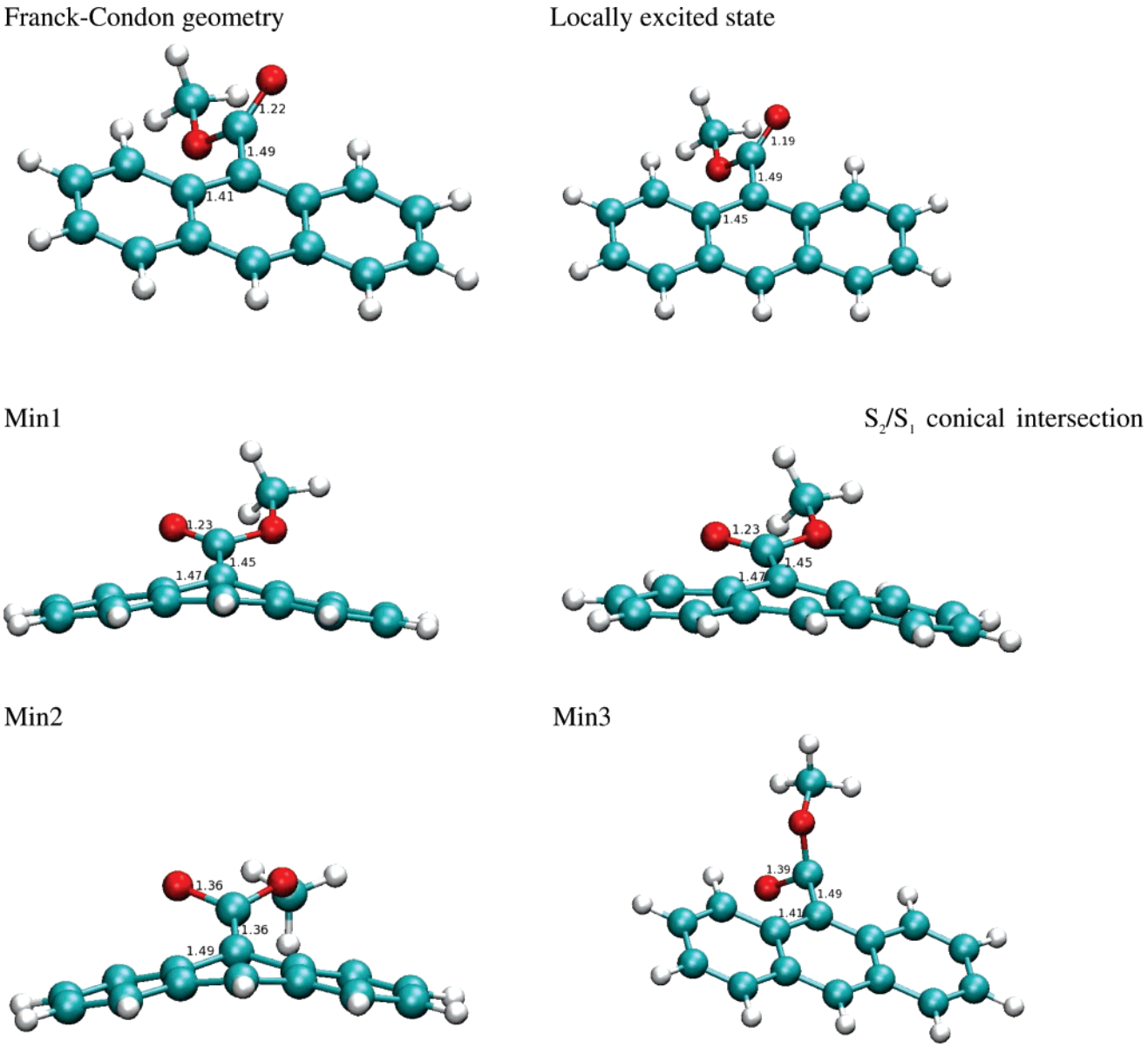

Figure 6. Important structures in the S_1 state of 9-methylanthroate. The Franck−Condon geometry has been obtained as a ground-state minimum using the MP2/6-31g* method; all of the excited-state minima and the S_2/S_1 conical intersection have been obtained by the CAS-SCF 6/6 method using the same basis.

a double one. The O═C−C_{anthr}−C dihedral angle is close to zero; however the carboxyl group is not coplanar with the anthracene ring because of its distortion. We have also found a structure originally suggested by Werner with a double bond between the anthracene ring and the carboxyl part (Min2). This state is, however, dominated by an excitation within the carboxylic group. The anthracene ring is bent in a similar way as found for a Min1 structure. We have also localized a third minimum on the S_1 potential with a planar ring geometry, elongated C═O bond, and pyramidilized carboxylic carbon (Figure 6). The two latter structures are energetically close to the LE state. However, the transition dipole moment is much smaller than that of Min1. Also the dipole moments of these structures are rather similar in the S_0 and S_1 states. This does not exclude the possibility that they contribute to the fluorescence spectra; structures of this type can be the source of the second peak observed in the experiment. Note that these states are energetically close to higher states with much larger transition dipole moments. The fact that the emission spectrum does not possess the mirror relation with the absorption spectrum even in nonpolar solvents suggests that the above states or at least some of them (presumably the state of C═O $\pi\pi^*$ character) might be responsible for the second, more energetic peak in nonpolar solvents.

We can, therefore, conclude that the following mechanism is likely to take place

$$S_0 \rightarrow S_1(FC) \rightarrow LE \rightarrow CT \text{ state}$$

$$LE \rightarrow \text{other distorted emitting states}$$

While the motion toward the locally excited minimum is essentially barrierless, the opposite is true for the second process. The intramolecular relaxation can thus take much longer times than was originally expected. We discuss this issue in section 3.5. Note that the conical intersection between the S_2 and the S_1 states (found from the locally excited minimum) has a geometry somewhere between the locally excited minimum and structure Min1. This intersection is energetically close to the locally excited state, suggesting that there will be only a small barrier for the escape from the locally excited state.

3.4. Temperature Scans. To validate the conclusions drawn from the theoretical simulations, we have performed temperature scans in heptane (Figure 4A) and in an ethanol−methanol mixture (Figure 4B). With decreasing temperature both polarity and viscosity are increasing. This interplay leads to a nonmonotonous dependence of the solvent shift on the temperature. With the ethanol−methanol mixture we can reach a glassy state that completely freezes most of the short time conformational dynamics.

In the case of the ethanol−methanol mixture the temperature decrease from 300 to 200 K leads to a gradual red shift of the fluorescence, probably due to the increase of solvent polarity and consequent higher stabilization of the states possessing a charge-transfer character. In addition, solvent relaxation is likely to contribute to the red shift since at these temperatures SR still occurs on faster time scales than the intrinsic fluorescence. Moreover, no changes in the shape of the spectra are observed. At 150 K, the viscosity increase makes the formation of the states with a CT character difficult, and the fluorescence from the LE state prevails. Thus, a blue-shifted steady-state emission spectrum is observed. At 100 K, a polar glass is formed, which makes the solvent molecules immobile, preventing any change in the dye conformation as well as solvent relaxation. Therefore, an emission spectrum, which is supposed to be in shape and energy comparable to that of a Franck−Condon type, is observed (Figure 4B). This spectrum is blue-shifted, and the vibrational structure is visible. To find out to what extent solvent polarity influences the emission spectra in a glass system, we performed a temperature scan in a solvent with a significantly lower polarity (2-methyltetrahydrofurane). No significant difference in comparison to the spectra recorded in the ethanol−methanol mixture was observed (data not shown here).

A different picture is observed for a nonpolar solvent such as heptane. The decrease in temperature does not lead to any important spectral shift. With decreasing temperature the contribution from the more energetic excited states starts to dominate over the lower-energy charge-transfer state.

3.5. Time-Resolved Emission Spectra. The crucial point for quantitative SR studies presents the determination of "time 0 spectrum", i.e., the spectrum emitted prior to any change of the position and orientation of the solvent molecules ("Franck−Condon state"). The approximate procedure consists of subtracting the maximum of the absorption spectrum measured in the investigated system from the difference between the maxima of absorption and the emission spectra measured in a reference nonpolar solvent. For a precise description of this procedure, see a previous publication by Fee et.al.[31] Unfortunately, this approach fails in the case of the AS dyes. The above-mentioned intramolecular process introduces an additional photophysical effect in the reference nonpolar solvent. A wide range of molecules at various states contributes to the emission, which disables a simple determination of the steady-state maximum of the non-relaxed state. Thus, an alternative method must be used to obtain a reasonable "time 0 estimate". As shown above (Table 1), the absorption and excitation spectra are rather independent of both the position of attachment of the anthroyloxy group and the solvent used. Consequently, also the "time 0 spectrum" can be considered as to be almost invariant of those parameters.

It has been shown that the emission spectrum at the glassy state serves as a good approximation for "time 0 estimate" in a given solvent.[31] Moreover, the average frequency of those low-temperature spectra appears to be rather independent of the choice of solvent and position of attachment of the anthroyloxy

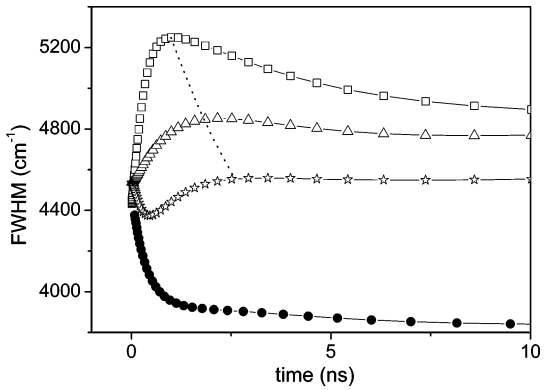

Figure 7. Full width at half-maximum time profiles of AS dyes in POPC LUVs (empty symbols) and paraffin oil (solid symbols): squares, 2-AS; triangles, 9-AS; stars, 16-AP; circles, 2-AS in paraffin oil. The dashed line illustrates the shift of the maxima toward longer times in the sequence 2-AS < 9-AS < 16-AP.

group (e.g., $\upsilon_{av} = 23\,840$ cm^{-1} and $\upsilon_{av} = 23\,800$ for 16-AP in EtOH + MetOH glass and 2-AS in 2-MTHF glass, respectively). Considering those arguments, we believe that the determined υ_{av} value of 23 800 cm^{-1} for 2-AS in 2-MTHF glass can be taken as a good estimate of the emission maximum of the Franck−Condon state of these AS dyes in POPC LUVs. Taking into consideration that the maximum of the excitation and absorption spectra of those dyes in LUVs differs at the most by 200 cm^{-1} from the spectrum in heptane (Table 1) and that the absolute value of the determined Stokes shifts in LUVs is about 2300 cm^{-1}, the maximal systematic error caused by the present "time 0 estimation" is lower than 10%. Thus, a "time 0 value" of 23 800 cm^{-1} is considered as a valuable estimate and serves further as an input value for constructing the correlation functions $C(t)$.

As concluded above from the steady-state emission data, a number of different states contribute to the photophysical behavior of *n*-AS dyes. Emission from different states takes place in nonpolar environments; however, the emission from the state with a CT character seems to dominate in polar systems. Naturally, solvent relaxation is present as well. These conclusions are also supported by the recorded TRES. A valuable parameter obtained by TRES is the time evolution of the fwhm. The pure solvent relaxation process is characterized by an increase at initial times followed by a decrease of the fwhm.[5,21,32] Such a behavior is clearly observed for 2-AS (Figure 7). When more processes take place the time course of the fwhm naturally becomes more complex, which is the case for 16-AP (Figure 7). The steep decline at the very early times (up to 1 ns) indicates that an additional process, which is not fully captured with the given time resolution, occurs. The origin of the complex behavior of 16-AP will be discussed further in the text.

The fwhm time profile can also serve as a rough estimate of the kinetics of the solvation dynamics. Logically, the maximum of the fwhm time dependence is shifted to the shorter times when the relaxation process gets faster. This behavior of fwhm-(t) is nicely illustrated for dye Patman embedded in POPC LUVs measured at various temperatures (Figure 8). Patman is reported to show a pure solvent relaxation response in the fluid phase of a phospholipid bilayer.[5] Obviously, the faster SR kinetics, i.e., the shorter the solvent relaxation time τ_{SR}, the shorter times correspond to the maxima of fwhm(t) (Figure 8). The fwhm time profiles of AS dyes in POPC LUVs show similar trends, and the maxima of the slower processes are shifted to shorter times in the sequence 16-AP > 9-AS > 2-AS (see dashed line

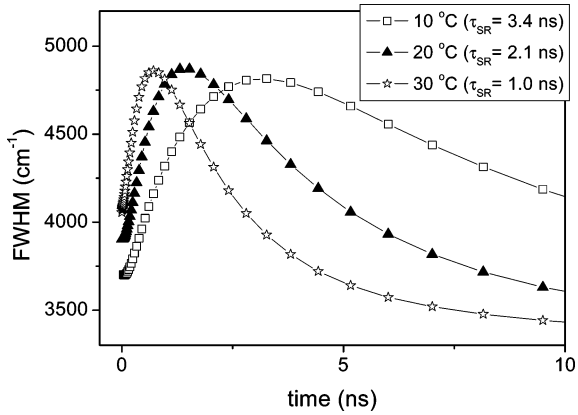

Figure 8. Full width at half-maximum time profiles of Patman in POPC LUV fors 10 °C (squares), 20 °C (triangles), and 30 °C (stars). The maxima of the fwhm's are shifted to the shorter times as the solvent relaxation becomes faster. The kinetics of solvent relaxation are described by solvent relaxation time τ_{SR}. Its values are 3.4, 2.1, and 1.0 ns for 10, 20, and 30 °C, respectively.

TABLE 4: Characteristics Obtained by Analyzing Correlation Functions in POPC LUVs and in Paraffin Oil[a]

	ν_{t0} (cm^{-1})	$\Delta\nu$ (cm^{-1})	τ_r[b] (ns)	% observed
2-AS[c]	23 800	2950	1.61	85
9-AS[c]	23 800	2450	1.40	73
16-AP[c]	23 800	2300	0.62	37
2-AS[d]	23 800	1630	0.58	44

[a] ν_{t0} corresponds to the spectral maximum of "time 0 estimate", $\Delta\nu$ is the overall Stokes shift, and % observed stands for the amount of the relaxation process that was captured with a given time resolution (30 ps). The percentage observed is obtained by comparing the values gained by the "time 0 estimation" and the first value of the TRES maximum $\nu(0)$ obtained by the "spectral reconstruction". [b] The integral relaxation time characterizes the overall relaxation process and provides only limited information on the individual processes, i.e., intramolecular relaxation and solvent relaxation. [c] In POPC LUVs. [d] In Paraffin oil.

in Figure 7). It indicates that the nanosecond relaxation process seems to accelerate when approaching the bilayer interface. In addition, the fwhm time profile obtained for the paraffin oil is almost constant on the nanosecond time scale, and only the rapid decline of the fwhm at the initial times is detected. Thus, it can be concluded that the water molecules that are absent in the paraffin oil and present in the bilayer are actually responsible for the slow nanosecond relaxation of AS dyes.

Another important parameter yielded by the TRES analysis is the overall Stokes shift that characterizes the micropolarity of the dye microenvironment. This also holds true for AS dyes featuring complex photophysics. As evident from Table 4, the Stokes shift, proportional to micropolarity, decreases with deeper location of the chromophore. Interestingly, even though the 2-AS and 9-AS dyes are reported to be located close to each other,[10] a large change in $\Delta\nu$ is observed. This fact supports the idea of a steep change in water density along the *z*-axes in the carbonyl region of the bilayer.[9,33] The comparison to the data measured in the paraffin oil, where the smallest $\Delta\nu$ was observed, evokes that water molecules are also present in the microenvironment of 16-AP. It means that either 16-AP is not buried as deep in the backbone region as reported previously[10] or that the chromophore itself perturbs the bilayer to the extent that water molecules can penetrate deeper. Alternatively, a significant dipole moment of the chromophore in the excited state may draw the water molecules via dipole−dipole interaction from the bilayer interface toward the backbone region of the bilayer.

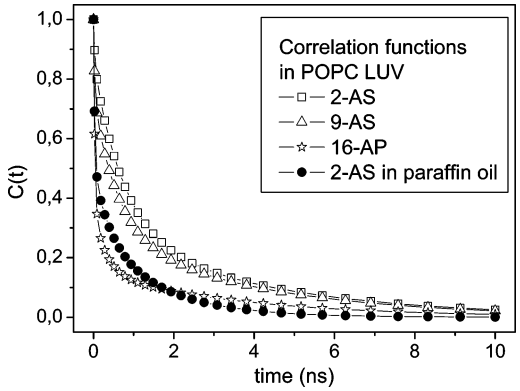

Figure 9. Correlation functions of AS dyes in POPC LUVs (empty symbols) and paraffin oil (solid symbols): squares, 2-AS; triangles, 9-AS; stars, 16-AP; circles, 2-AS in paraffin oil.

Parallel trends are found for the preferential solvation in mixtures of two liquids.[34]

By visual inspection of the correlation functions (Figure 9), by comparison of the integral relaxation times τ_r (Table 4), as well as by the amount of the relaxation process captured with the given time resolution (Table 4), it is evident that with the deeper location of the AS dyes in the bilayer the relaxation becomes faster on the whole. In the case of 2-AS, the observed behavior is similar to that of the dyes that undergo relaxation process mostly via nanosecond solvent relaxation and are located at the headgroup region.[5,35,36] Moreover, the integral relaxation time is in the range of 2 ns, implying that 2-AS occupies a similar region and features a similar solvation behavior as the already reported headgroup probes, for instance, Patman.[5] In contrast to 2-AS, 16-AP shows more complex behavior. The fwhm time profile appears to be nontrivial, and only 35% of the relaxation process is captured with the given time resolution. The reason is that a fast relaxation process dominates over the solvation response in the nonpolar environment of the backbone region. Such a conclusion is supported by the data measured in the paraffin oil, which serves as a feasible model system to the bilayer backbone. Obviously, only a minor part of the relaxation process is also captured with the given time resolution in the paraffin oil, and the relaxation times are on the same order as in the case of 16-AP embedded in POPC LUVs. The slightly slower relaxation time and the higher amount of the observed solvent relaxation can be ascribed to the larger viscosity of the paraffin oil compared to that of the backbone region of the bilayer.[37,38]

3.6. Dynamics of the *n*-AS Solvation and Intramolecular Relaxation. The experimental data indicate that the relaxation process of AS dyes in phospholipid bilayers is rather complex. The TRES reflect both intramolecular and intermolecular dynamics. The intramolecular relaxation includes torsional relaxation, formation of a charge-transfer state, and also other rearrangements of the carboxylic moiety leading to nonpolar emitting states. At the same time, solvent relaxation takes place. These two processes cannot be completely separated from each other. The rate of the LE → CT transition will most certainly depend on the polarity of the dye microenvironment. The time scale for the faster components of the solvent relaxation (libration, rearrangement, etc.) is roughly comparable with that of the intramolecular relaxation. We believe, however, that the intramolecular relaxation occurs on a subnanosecond time scale. This is supported by results of ab initio calculations. The intersection between the locally excited state and the charge-transfer state occurs only 0.2 eV above the locally excited minimum. The transition state leading to the CT state is thus

energetically well accessible, and the rate of this transition is only limited by intramolecular energy transfer between modes. The same holds true for the transition to the other emitting states.

We can conclude that the slowest process observed in the time-resolved fluorescence spectra corresponds to the diffusion part of solvent relaxation. The use of *n*-AS dyes is, therefore, justified for solvation studies of phospholipids bilayers where the diffusion-driven solvent relaxation plays a dominant role. From the results of the time-resolved experiments the following conclusions about the solvation dynamics in the lipid bilayers can be drawn. First, as we go deeper into the bilayer the solvation contribution to the response functions becomes less significant but does not disappear completely even for the most buried 16-AP. Second, the time dependence of fwhm indicates that the solvent relaxation becomes slower upon approaching the center of the bilayer. What we observe is essentially preferential solvation in a mixture of a polar and nonpolar solvents. While the nonpolar solvent (in our case fatty acid chains) does not contribute significantly to the Stokes shift, the polar molecules (water in our case) contribute more or less proportionally to the number of surrounding solvent molecules. With decreasing water concentration we observe a decreasing Stokes shift, and the solvation process becomes longer.[39] If we considered the diffusion constant to be independent of the distance from the bilayer head, then we should in principle be able to reconstruct the water concentration profile. Unfortunately, our data at this point are too noisy for such a reconstruction. The obtained data, however, qualitatively support the results of molecular dynamical simulations. These are showing a steep decrease of water concentration from the headgroup to the backbone region of the bilayer.[40] A certain amount of water is, however, always present even in the microenvironment of the 16-AP, which is supposed to be buried in the backbone region.[10] Note also that the headgroup region of the bilayer is coarse and that the water profile reflects mostly the roughness of the surface.

4. Conclusions

We have explored the nature of light-emitting states of *n*-AS dyes by combining fluorescence spectroscopy with quantum chemical calculations. The recorded time-resolved emission spectra revealed a nontrivial behavior of these dyes in the backbone region of the phospholipid bilayer, showing the presence of multiple relaxation processes. Thus, steady-state fluorescence spectra were recorded in systems of varying viscosities and polarities to elucidate the *n*-AS photophysics. In addition, quantum chemical calculations have been performed for a model 9-methylanthroate dye. Combining these two approaches, we have shown that the mere relaxation to the locally excited state after the primary excitation cannot account for the experimentally observed behavior. Existence of an emitting state of a charge-transfer character was, therefore, suggested and confirmed by means of high-level ab initio calculations. We have also estimated the barrier between the locally excited state and the other emitting states. Time-resolved experiments have been discussed focusing on these new photophysical findings. We have concluded that time-resolved fluorescence measurements using the *n*-AS dye can serve as a valuable source of information on the diffusion-controlled part of solvent relaxation, while processes on femtosecond and picosecond time scales reflect in a rather complex way also intramolecular relaxation of the chromophore.

Acknowledgment. We thank the Grant Agency of the Academy of Sciences of the Czech Republic for support via Grant No. A400400503. This work also has been supported by the Czech Ministry of Education (Grant Nos. LC512 and LC06063). P.S. also thanks the Grant Agency of the Czech Republic for Postdoctoral Grant No. 203/07/P449.

References and Notes

(1) Milhaud, J. *Biochim. Biophys. Acta* **2004**, *1663*, 19.
(2) Wiener, M. C.; King, G. I.; White, S. H. *Biophys. J.* **1991**, *60*, 5610.
(3) Wiener, M. C.; White, S. H. *Biophys. J.* **1992**, *61*, 4210.
(4) Bursing, H.; Ouw, D.; Kundu, S.; Vohringer, P. *Phys. Chem. Chem. Phys.* **2001**, *3*, 23710.
(5) Sýkora, J.; Kapusta, P.; Fidler, V.; Hof, M. *Langmuir* **2002**, *110*, 571.
(6) Hutterer, R.; Schneider, F. W.; Sprinz, H.; Hof, M. *Biophys. Chem.* **1996**, *61*, 151.
(7) Jurkiewicz, P.; Olzyńska, A.; Langner, M.; Hof, M. *Langmuir* **2006**, *22*, 10741.
(8) Forrest, L. R.; Sansom, M. S. P. *Curr. Opin. Struct. Biol.* **2000**, *10*, 174.
(9) Zubrzycki, I. Z.; Xu, Y.; Madrid, M.; Tang, P. *J. Chem. Phys.* **2000**, *112*, 3437.
(10) Abrams, F. S.; Chattopadhyay, A.; London, E. *Biochemistry* **1992**, *31*, 5322.
(11) Villalain, J.; Prieto, M. *Chem. Phys. Lipids* **1991**, *59*, 9.
(12) Werner, T. C.; Hoffman, R. M. *J. Phys. Chem.* **1973**, *77*, 1611.
(13) Berberan-Santos, M. N.; Prieto, M. J. E.; Szabo, A. G. *J. Phys. Chem.* **1991**, *95*, 5471.
(14) Hutterer, R.; Schneider, F. W.; Lanig, H.; Hof, M. *Biochim. Biophys. Acta* **1997**, *1323*, 195.
(15) Chattopadhyay, A.; Mukherjee, S. *Langmuir* **1999**, *15*, 2142.
(16) Maroncelli, M. *J. Mol. Liq.* **1994**, *57*, 1.
(17) Michael, D.; Benjamin, I. *J. Chem. Phys.* **2001**, *114*, 2817.
(18) Cichos, F.; Brown, R.; Rempel, U.; von Borczyskowski, C. *J. Phys. Chem. A* **1999**, *103*, 26506.
(19) Tamashiro, A.; Rodriguez, J.; Laria, D. *J. Phys. Chem. A* **2002**, *106*, 215.
(20) Hope, M. J.; Bally, M. B.; Mayer, L. D.; Janoff, A. S.; Cullis, P. R. *Chem. Phys. Lipids* **1986**, *40*, 89.
(21) Horng, M. L.; Gardecki, J. A.; Papazyan, A.; Maroncelli, M. *J. Phys. Chem.* **1995**, *99*, 17311.
(22) Granucci, G.; Toniolo, A. *Chem. Phys. Lett.* **2000**, *325*, 79.
(23) Werner, H. J.; Knowles, P. *Molpro*, version 2002.6.
(24) Stewart, J. J. P. *Mopac 2000*; Fujitsu Limited: Tokyo, Japan, 1999.
(25) Turro, N. J. *Modern Molecular Photochemistry*; University Science Books: Sausalito, CA, 1991.
(26) Werner, T. C.; Hercules, D. M. *J. Phys. Chem.* **1969**, *73*, 2005.
(27) Werner, T. C.; Matthews, T.; Soller, B. *J. Phys. Chem.* **1976**, *80*, 533.
(28) Swayambunathan, V.; Lim, E. C. *J. Phys. Chem.* **1987**, *91*, 6359.
(29) Matayoshi, E. D.; Kleinfeld, A. M. *Biophys. J.* **1981**, *35*, 215.
(30) Dey, J.; Haynes, J. L.; Warner, I. M.; Chandra, A. K. *J. Phys. Chem.* **1997**, *101*, 2271.
(31) Fee, R. S.; Maroncelli, M. *Chem. Phys.* **1994**, *183*, 235.
(32) Richert, R. *J. Chem. Phys.* **2001**, *114*, 7471.
(33) Nagle, J. F.; Tristram-Nagle, S. *Biochim. Biophys. Acta* **2000**, *1469*, 159.
(34) Petrov, N. K. *High Energy Chem.* **2006**, *40*, 22.
(35) Dutta, P.; Sen, P.; Mukherjee, S.; Bhattacharyya, K. *Chem. Phys. Lett.* **2003**, *382*, 426.
(36) Halder, A.; Sen, S.; Das Burman, A.; Patra, A.; Bhattacharyya, K. *J. Phys. Chem. B* **2004**, *108*, 2309.
(37) Mateo, C. R.; Lillo, M. P.; Brochon, J. C.; Martlnez-Ripoll, M.; Sanz-Aparicio, J.; Acuiia, A. U. *J. Phys. Chem.* **1993**, *97*, 3486.
(38) Lopez, Cascales, J. J.; Huertas, M. L.; de la Torre, J. G. *Biophys. Chem.* **1997**, *69*, 1.
(39) Agmon, N. *J. Phys. Chem. A* **2002**, *106*, 7256.
(40) Jadlovszky, P.; Mezei, M. *J. Chem. Phys.* **1999**, *111*, 10770.